Catalysis Today 394-396 (2022) 25–33

Contents lists available at ScienceDirect

Catalysis Today

journal homepage: www.elsevier.com/locate/cattod

Role of alkali-cyano group interaction in g-C_3N_4 based catalysts for hydrogen photo-production

Uriel Caudillo-Flores [a,b], Alejandro Ares-Dorado [a], Gabriel Alonso-Nuñez [b], David Tudela [c], Marcos Fernández-García [a,*], Anna Kubacka [a,*]

[a] Instituto de Catálisis y Petroleoquímica, CSIC, C/Marie Curie 2, 28049 Madrid, Spain
[b] Universidad Nacional Autónoma de México, Centro de Nanociencias y Nanotecnología, Km. 107 carretera Tijuana-Ensenada, C.P. 22800 Ensenada, Baja California, Mexico
[c] Departamento de Química Inorgánica, Facultad de Ciencias, Universidad Autónoma de Madrid, 28049 Madrid, Spain

ARTICLE INFO

Keywords:
Carbon nitride
Alkali
Photo-catalysis
Hydrogen
Sunlight

ABSTRACT

Carbon nitride based materials incorporating K and Na alkali ions were used as support(s) to deposit platinum. The systems were tested in the photo-production of hydrogen using methanol as a sacrificial molecule. Tests under UV and sunlight-type illumination conditions showed an important promoting effect of the alkali ions irrespective of the illumination source characteristics. The measurement of the quantum efficiency was used to quantitatively assess the performance of the catalysts. Outstanding results were obtained, particularly under sunlight illumination. A complete characterization study of the materials was carried out to establish a structure-activity link. This link correlates catalytic activity with the capture of charge carrier species by surface cyano groups directly associated with the presence of alkali ions at the carbon nitride component.

1. Introduction

One of the modern materials showing high potential for photo-catalytic applications corresponds to the graphite-like carbon nitride (g-C_3N_4). Graphitic carbon nitride consists of a graphite-like structure of tris-z-triazine layers connected through amino groups [1,2]. As discussed in previous works, excellent electronic and chemical properties as well as significant thermal stability have triggered the use of g-C_3N_4-based single or composite materials as catalysts for many photochemical reactions [3,4]. The activity of carbon nitride materials is commonly promoted with the help of metals such as Ag, Au, Pd or Pt [5–7]. Among them, Pt-promoted semiconductors (and, particularly carbon nitride) systems appears as a central catalyst that would find utility for specific novel processes such as hydrogen production, particularly using a free ("zero-cost") energy source such as the sun [2,8]. However, as happens with all photo-catalysts, the Pt-g-C_3N_4 system requires improvement of its photo-catalytic properties upon all (UV and visible) illumination conditions and a potential pathway corresponds to the doping of the carbon nitride semiconductor. Specifically, in the case of Pt-g-C_3N_4 materials, alkali doping (mostly using K and Na) has been shown rather effective in promoting UV but also visible light activity [1,2,4]. This has been ascribed to a multitude of physico-chemical factors including effects in light absorption by bang gap decrease (i.e. increasing visible light absorption), charge capture at surface positions and charge recombination. Within this context, the appearance of specific surface groups (mostly cyano groups, localizing charge) at carbon nitride external layers has shown to positively interact with alkali (Na) doping, affecting charge (electron) capture and recombination and boosting significantly photo-catalytic activity [1,9,10].

This work aims to analyze the production of hydrogen from bio-alcohols by Pt-loaded K/Na-containing carbon nitride materials. To examine activity performance we measured and analyzed the quantum efficiency values under UV and visible illumination conditions [11]. The interplay between surface groups and alkali doping in Pt-g-C_3N_4 powders is addressed here from a novel perspective, attempting to establish a structure-activity link that would unravel the physical origin of the photo-activity.

2. Materials and methods

The g$C3N_4$ based materials were prepared by thermal polymerization of physical mixtures of dicyandiamide (Aldrich, 99%) and

* Correspoding authors.
E-mail addresses: mfg@icp.csic.es (M. Fernández-García), ak@icp.csic (A. Kubacka).

https://doi.org/10.1016/j.cattod.2021.06.028
Received 9 February 2021; Received in revised form 11 May 2021; Accepted 25 June 2021
Available online 14 July 2021

Potassium nitrate or Sodium bicarbonate (Aldrich, 99% and 99.5% respectively). First, 10 g dicyandiamide were dissolved in water. Then, the desired amount of KNO_3 or $NaHCO_3$ was added to the dicyandiamide solution, heated, stirred and dried at 80 °C. The dry product was put in a muffle and heated to 550 °C for 2 h. After grinding, a similar second calcination step was carried out but in this case at 500 °C. A gC_3N_4 reference was obtained following the previously described process without adding the alkali precursor(s). The co-catalyst was introduced by a deposition method using a H_2PtCl_6 (Aldrich) solution. First, the sample was suspended by stirring in a deionized water solution for 30 min. After that, the proper quantity of H_2PtCl_6 was added to the solution (to get throughout the series a constant 0.4 mol. % of Pt on metal basis) and kept stirring for 5 min more. The reduction was carried out using a $NaBH_4$ (Aldrich) aqueous solution (Pt/$NaBH_4$ molar ratio 1/5). The final solid was profusely rinsed with deionized water, collected by centrifugation and dried at 80 ^{0}C. Chemical analysis (measured using atomic emission with inductive coupled plasma (ICP-AES) using an Optima 3300DV Perkin Elmer spectrometer) provided a K/Na and platinum content corresponding to the nominal ones of the samples with an error of 3.6/2.9% and 2.4%, respectively. So, the samples were labeled as Pt/xK-gC_3N_4 or Pt/xNa-gC_3N_4 with x being the K/Na molar content (%) of the synthesis. A Pt/ gC_3N_4 reference catalyst was also studied.

2.1. Characterization methods

The BET surface areas and average pore volumes and sizes were measured by nitrogen physisorption (Micromeritics ASAP 2010). XRD profiles were obtained using a Seifert D-500 diffractometer using Ni-filtered Cu Kα radiation with a 0.02° step. The particle sizes were estimated using XRD using the Williamson–Hall formalism [12]. UV–vis diffuse-reflectance spectroscopy experiments were performed on a Shimadzu UV2100 apparatus using nylon as a reference and the results presented as Kubelka-Munk transform [13]. Band gap analysis for the gC_3N_4 indirect gap semiconductor was performed following standard procedures; e.g., plotting $(h\nu a)^n$ (n = ½ or 2 for indirect or direct semiconductor; $h\nu$ = excitation energy, a = absorption coefficient) vs. energy and obtaining the corresponding intersection of the linear fit with the baseline [14]. Transmission electron microscopy (HRTEM) images were recorded on a JEOL 2100F TEM/STEM microscope. Particle size distributions of the noble metal were obtained counting more than 250 particles in all cases. XPS data were recorded on 4 × 4 mm^2 pellets, 0.5 mm thick, prepared by slightly pressing the powered materials, which were outgassed in the prechamber of the instrument at room temperature up to a pressure $<2 \times 10^{-5}$ Pa to remove chemisorbed water from their surfaces. The XPS spectra of the samples were recorded using a SPECS® spectrometer with a PHOIBOS® 150 WAL hemispherical energy analyzer with angular resolution (<0.5 degrees), equipped with an XR 50 Al-X-ray and μ-FOCUS 500 X-ray monochromator (Alexcitation line) sources. Samples were first degassed at 10^{-5} mbar in the pretreatment chamber before being transferred to the analysis chamber, where residual pressure was kept below 5×10^{-9} mbar during data acquisition. The binding energies (BE) were referenced to the C 1s peak (284.8 eV) to account for charging effects. Surface chemical compositions were estimated from XP-spectra, by calculating the integral of each peak after subtraction of the "S-shaped" Shirley-type background [15] using the appropriate experimental sensitivity factors and the CASA-XPS (version 2.3.15) software.

2.2. Photo-catalytic experimental and computational details

Gas-phase reaction was carried in a continuous flow annular photoreactor containing ca. 0.3 mg cm^{-2} of photocatalyst as a thin layer coating on a pyrex tube. The scheme of the reactor is shown in Fig. S1 of the Supporting information section. After degassing the line with Ar, the flow was settled down to 10 mL min^{-1} and stabilized before reaction. A 3:7 MeOH/H_2O mixture was achieved with a carrier having saturated water content. Water was injected with a syringe pump and the corresponding methanol content using a saturator at controlled temperature. Photocatalytic experiments were carried out under UV-A light irradiation (Philips BLB F6T5; 6 W) or sunlight irradiation (Philips TL54–765; 6 W). In both cases, four fluorescent lamps symmetrically positioned outside the photo-reactor were used (see configuration at Supporting information section, Fig. S1, Section 1). Reaction rates for hydrogen production were evaluated under steady-state conditions, typically achieved after ca. 2 h from the irradiation starting. The concentration of the reactants was analyzed using an online gas chromatograph (Agilent GC 6890) equipped with HP-PLOT-Q/HP-Innowax columns (0.5/0.32 mm I.D. × 30 m) and thermal conductivity and flame ionization detectors. The absence of catalytic changes was confirmed in the following 24 h of operation.

Considering that two electrons are required to reduce two protons and thus to produce one H_2 molecule, the Quantum Efficiency is calculated as Eq. 1, dividing the reaction rate (r: mol m^{-2} s^{-1}) with the averaged superficial rate of photon absorption ($< e^{a,s} >$: Einstein m^{-2} s^{-1}) [[11]. Details of the calculation are presented in Section 1 (Reaction set-up and Quantum Efficiency) of the Supporting information file and fully described in Refs. [16,17].

$$\eta_q(\%) = 100 \times \frac{2xr}{< e^{a,s} >} \quad (1)$$

3. Results and discussion

The catalytic performance for hydrogen photocatalytic production is presented in Figs. 1 and S2 for the two illumination sources here utilized, UV and sunlight-type. Our materials show activity under both UV and visible illumination. The presence of alkali ions at the carbon nitride increases the activity significantly. This is observed as measured using the reaction rate and the quantum efficiency observables. Optimum activity is always reached using the sample with a nominal (initial) concentration of 4 mol. % of the alkali ion. Thus, in both series (K and Na) we can find an optimum alkali content maximizing activity under all illumination sources here studied. Stable operation of the most active samples for relatively long time on stream periods is shown in Fig. S2. As a quantitative measure of the enhancement with respect to the Pt/gC_3N_4 system, we can mention that K enhances the quantum efficiency by a factor 1.9/2.5 under UV/sunlight-type illumination, while the corresponding values for Na are 2.2/2.9 (Fig. 1). These measurements allow to quantify the quantum efficiency expected using the AM1.5 solar standard, a fact not feasible using the reaction rate nor the apparent quantum efficiency. Using the corresponding light intensity distributions of our illumination source and the AM1.5 standard [16], a strong promoting effect (with respect to the bare carbon nitride) of 2.4 (K) and 2.8 (Na) times is thus obtained.

In first place, the characterization of the materials attempted to analyze alkali ions presence in the carbon nitride based materials using ICP-AES. The real loading of the powders are presented in Fig. S3 of the Supporting information section. Linear correlations are obtained between theoretical (synthesis conditions) and real loadings of our materials. For the same initial (synthesis) alkali molar concentration, this figure allows to infer that the K (real) loading is lower than the one of Na by a nearly constant value of ca. 2.6 times. The size of the alkali ion would critically control the alkali loading process into the carbon nitride structure [18].

Fig. 2 displays the XRD patterns of the Pt/gC_3N_4 reference and the Pt/x(K/Na)-gC_3N_4 samples. All diffraction patterns show the typical profile of the graphitic C_3N_4 layered structure, dominated by the interlayer-stacking (002) reflection. Additionally, the (100) reflection, related to the intralayer structural packing motif of tri-s-triazine units, is detected in all samples at around 13.1 degrees [2,19]. Absence of significant changes in these two graphitic C_3N_4 XRD peaks can be noticed among samples. This suggests that the alkali-containing species do not

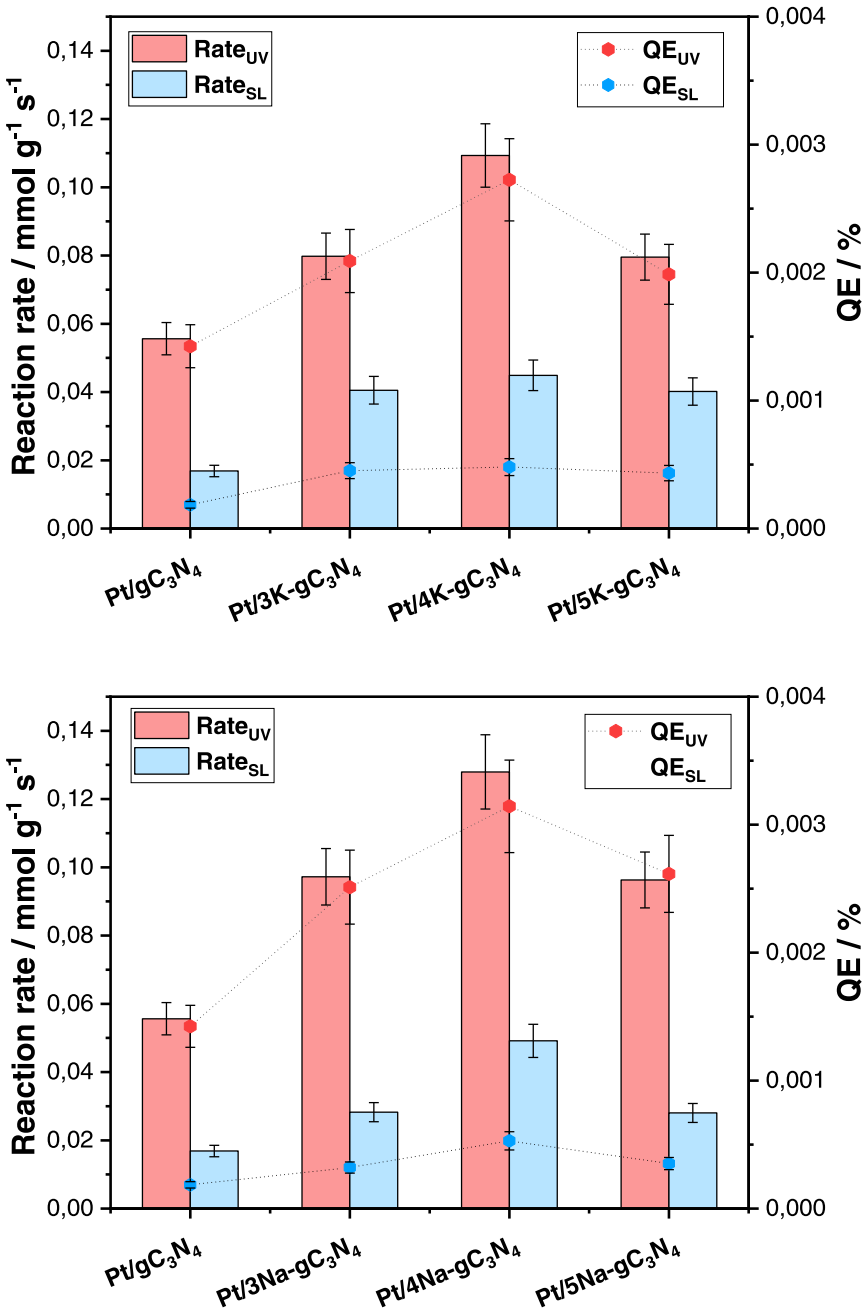

Fig. 1. Reaction rate and quantum efficiency for hydrogen photo-production using Pt/x-gC_3N_4 (x = K, Na) and Pt/gC_3N_4 reference materials. Results for UV and sunlight-type (SL) illumination conditions are presented.

alter to a significant degree the support's structural properties. The IR analysis (presented in Figs. 2, S4 and S5) also provides a similar conclusion. Fig. 2 also contains the IR spectra of the samples in the ca. 1800–800 cm^{-1} range. In this frequency region, we can observe peaks associated with stretching modes of CN heterocyclic moieties (ca. 1700–1200 cm^{-1}) and the distinctive breathing mode of tris-s-triazine (peak at ca. 815 cm^{-1}) [2,5]. Absence of differences among samples can be noticed, reinforcing the idea of the small structural changes originated by the presence of alkali atoms in the carbon nitride support.

The rather stable and non-perturbed structural properties of the carbon nitride component demonstrated by the combined XRD-IR analysis along the (alkali-containing) series of samples can be correlated with the similar morphological observables presented in Table 1 for all catalysts. In particular, the BET area of the reference sample is ca. 16 m^2 g^{-1} while those of the (alkali containing) samples oscillate between 16 and 17 m^2 g^{-1}. So, a near negligible variation of surface area as well as other morphological properties (pore size and volume, see Table 1) would take place and is likely attributable to a limited effect of alkali ions, indicating a marginal differential effect in the adsorption of the reactants with respect to the Pt/gC_3N_4 reference. These mild morphological effects appear independent of the nature of the alkali cation.

XPS renders information about the K and Na cations located at the support. The low quantity of K species (Fig. S3) complicates the characterization using XPS (see the poor signal presented in Fig. 3). We can only observe a broad bump in the XPS spectra of the corresponding samples. The signal intensity in the region between 292 and 293.5 eV is indicative of the K(I) chemical state [20,21], although we cannot ascertain its local environment. For Na we can see a 1s signal centered at 1071.5 eV, characteristic of Na(I) in carbon nitride based samples [20,

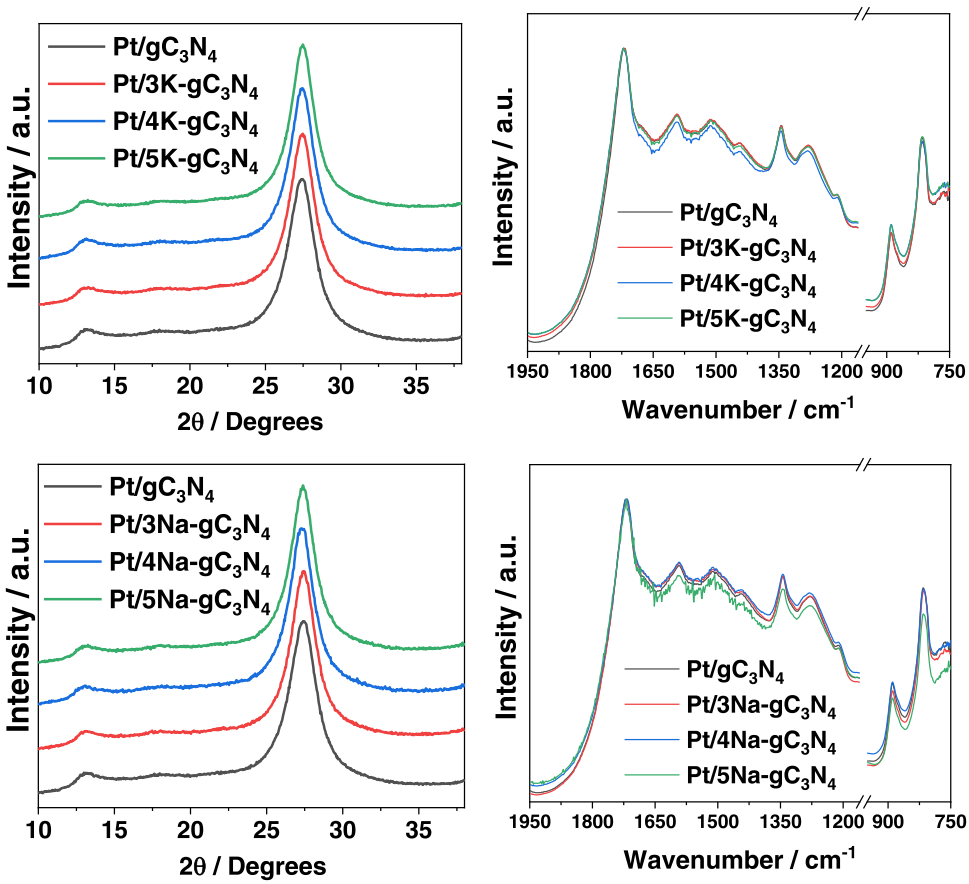

Fig. 2. XRD patterns and infrared spectra of Pt/x-gC_3N_4 (x = K, Na) and Pt/gC_3N_4 reference materials.

Table 1
BET surface area, pore volume, pore size and band gap values for initial (fresh) and post-reaction (post) samples[a].

Catalyst	BET surface area (fresh/post; m^2 g^{-1})	Pore volume (fresh/post; cm^3 g^{-1})	Pore size (fresh/post; nm)	Band Gap (fresh/post; eV)
Pt/gC_3N_4	16/17	0.066/0.066	21.7/21.8	2.67/2.68
Pt/3K-gC_3N_4	$16/16_{.5}$	0.070/0.069	21.3/21.3	2.66/2.67
Pt/4K-gC_3N_4	17/17	0.066/0.067	20.0/20.1	2.65/2.67
Pt/5K-gC_3N_4	17/17	0.059/0.060	17.2/17.1	2.65/2.66
Pt/3Na-gC_3N_4	16/16	0.070/0.069	23.4/23.2	2.68/2.64
Pt/4Na-gC_3N_4	$17/17_{.5}$	0.075/0.073	20.8/21.0	2.68/2.65
Pt/5Na-gC_3N_4	16/16	0.066/0.067	23.5/23.5	2.68/2.65

[a] Average Standard Error: BET surface area 1.6 m^2 g^{-1}; Band gap 0.03 eV.

21]. In this case, the higher quantity of alkali facilitates the detection of the signal. The case of K cannot be ascertained using XPS (see Fig. 3) but for Na the Na/(C+N) atomic ratio takes values of 0.15/0.20/0.24 at% for Pt/3Na-g-C_3N_4/ Pt/4Na-g-C_3N_4/Pt/5Na-g-C_3N_4. These values are rather low compared with those coming from chemical analysis (from the Na content of the Pt/xNa-g-C_3N_4 samples presented in Fig. S3 we can calculate Na/(C+N) values higher by 2.4–3.1 times). The important difference between the alkali content detected using XPS and chemical analysis clearly indicates the preferential presence of such cations at the bulk of the material. Due to the absence of changes in C/N XPS signals (results not shown), the alkali cations would be likely at interlayer positions (and not substituting C or N atoms at layer positions), interacting through electrostatic forces with the carbon nitride layers.

XPS was jointly used with microscopy to carry out the analysis of the supported metallic phase. Fig. 3 contains plots of the Pt 4*f* peak region for representative samples (most active K/Na-containing samples) under study. The fitting of the spectra showed the presence of metallic Pt ($4f_{7/2}$ at ca. 70.9 ± 0.2 eV for all samples), $Pt(OH)_2$ ($4f_{7/2}$ at ca. 72.3_5 ± 0.05 eV) and PtO ($4f_{7/2}$ at ca. 73.8_5 ± 0.05 eV) type species [20]. These platinum-containing species binding energies displayed rather similar values among all (present in Fig. 3 as well as other) samples. Also, a similar concentration of the corresponding Pt species is encountered in all catalysts, providing evidence of the equal (average) oxidation state of the noble metal throughout the series of samples. This fact would additionally indicate that the dominant Pt zerovalent phase (ca. 70% according to XPS) is surrounded by oxidized species, located at the external (surface and near surface) region of the noble metal particles.

Low and high magnified micrographs of the selected catalysts are presented in Fig. 4 for the most active Pt/x(K,Na)-gC_3N_4 samples. All materials show a finely dispersed metallic phase, homogeneously distributed over the typical laminar morphology of the support, the carbon nitride component. The particles have round, spherical shape. Analysis of platinum primary particle was carried out and the corresponding particle size distributions obtained are presented in Fig. S6 of the Supporting information. The average noble metal particle size takes a value of ca. 3.9 nm for the bare carbon nitride support, and takes values in the 3.9–4.3 nm range for the rest of the samples. This nearly constant average primary particle size value agrees well with the previous results of the noble metal dispersion obtained from XPS. Both techniques confirm the rather similar noble metal phase supported in our samples in terms of primary particle size and oxidation state. The

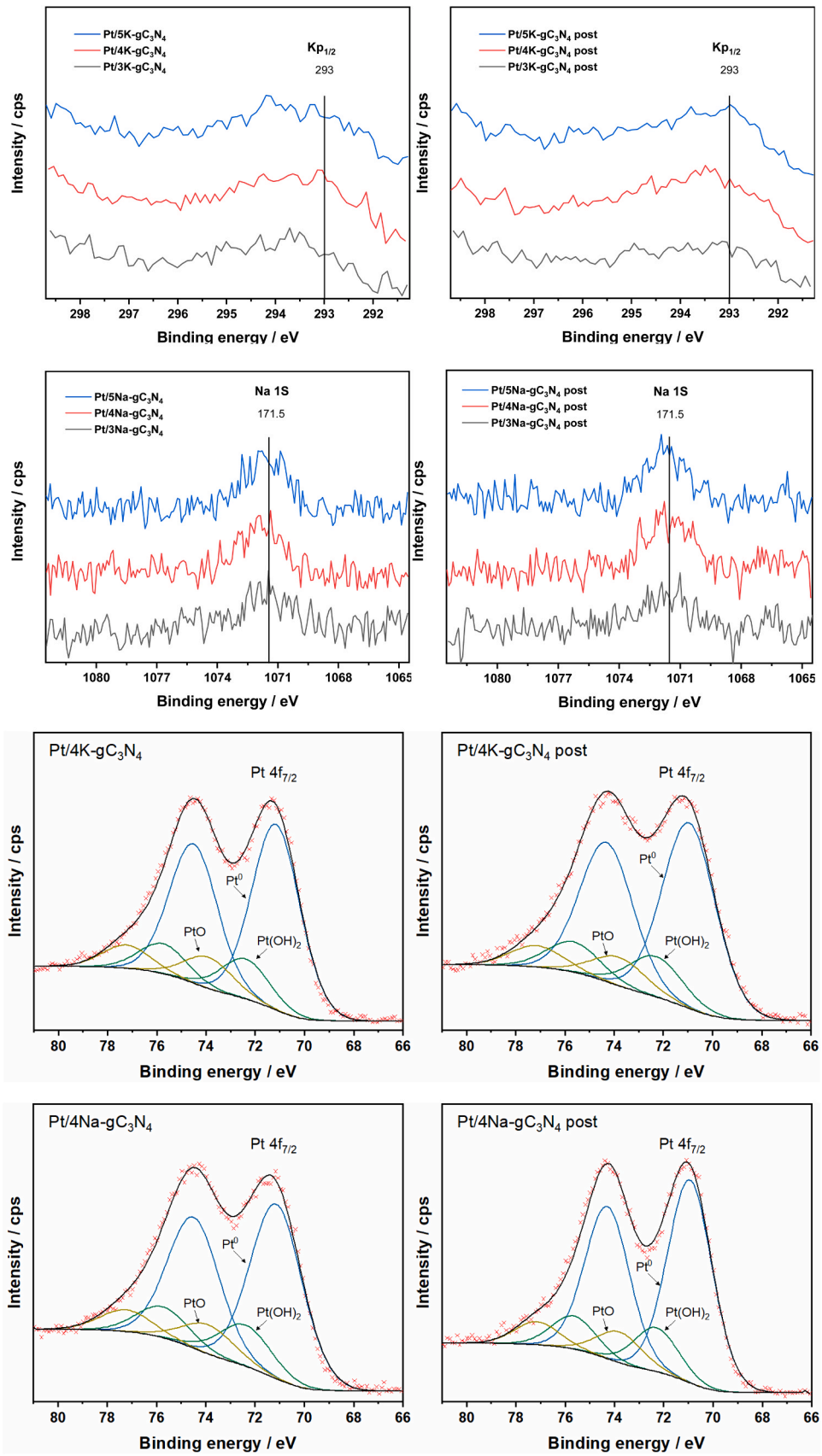

Fig. 3. K 2p, Na *1s,* Pt *4f* XPS spectra of selected Pt/X-gC_3N_4 materials (X = K,Na). Pre and post-reaction specimens are included.

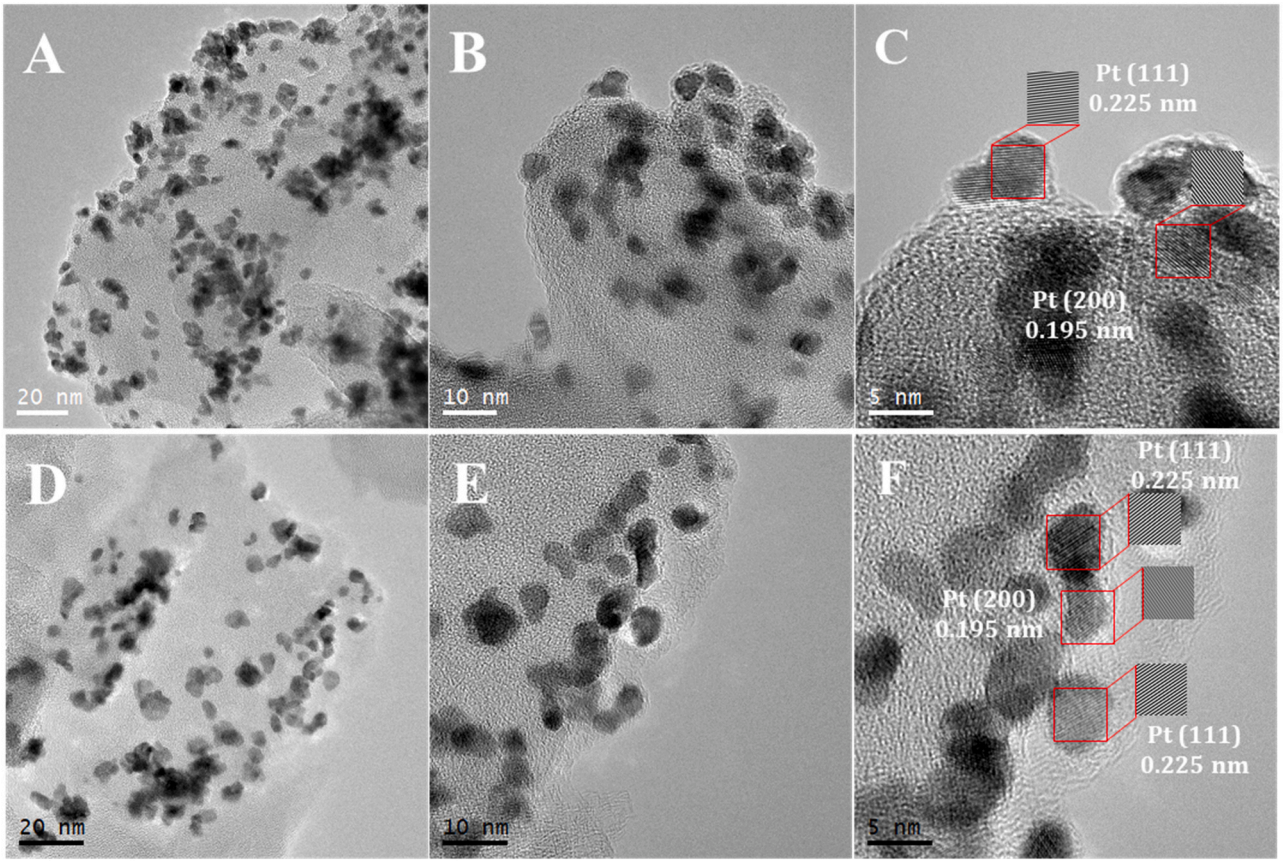

Fig. 4. Low and high magnification TEM micrographs of selected samples (A-C) Pt/4K-gC_3N_4; and (D-F) Pt/4Na-gC_3N_4.

characterization of the samples was completed with the analysis of the optical properties using UV–visible spectroscopy oxidation state (Fig. S7). Band gap values are all equal within the experimental error, with an average value of 2.65 eV, typical of the support [2,22]. The absence of band gap energy changes is also consistent with the absence of major structural changes (and particularly presence of defects) in the carbon nitride component [23]. Moreover, the joint analysis of band gap with the valence band edge measured using XPS showed that both the valence and the conduction bands of the materials only suffer minor changes among the samples of the series. The valence and conduction flat band potentials are thus equal among the samples of our series. Summarizing the physico-chemical characterization, the catalysts displayed rather similar structural, morphological and electronic properties of the noble metal and carbon nitride components. As discussed below, main differences appeared in the alkali-cyano group interaction.

In order to interpret photo-activity we initially utilized photoluminescence spectroscopy. Fig. 5 top and middle panels (A-D) correspond to the photoluminescence spectra of the powders under UV and visible excitation. Under UV the spectra show a single peak peaking at ca. 490 nm, with the typical asymmetric shape previously observed by many authors for carbon nitride based catalysts [2,5,22,24]. For visible excitation, we observed the presence of small intensity shoulders corresponding to defect states on top of the decay curve corresponding to the excitation [2,22,24]. Samples essentially differ in the intensity of the signal irrespective of the illumination wavelength. As the photoluminescence intensity is directly proportional to the recombination of charge after illumination, we can see that both alkali ions (K and Na) decrease significantly the recombination with respect to the Pt/gC_3N_4 reference system. A direct relationship can be established with the photoluminescence intensity (Fig. 5) and activity (Fig. 1). The minimum of photoluminescence intensity corresponds to the sample having maximum activity. Further increase of both K and Na leads to a less effective handling of charge carrier species and increasing photoluminescence intensity.

Some differences at the surface of the K and Na containing solids are also relevant in this context. Figs. S4 and S5 the vibrational spectra for the Pt/xK-gC_3N_4 and Pt/xNa-gC_3N_4 series of samples, respectively. OH/NH (ca. 3000–3600 cm^{-1}), carbonyl (ca. 1715 cm^{-1}) and cyano (ca. 2000–2250 cm^{-1}) groups are commonly observed at the surface of carbon nitride materials prepared with the same precursor(s) here used [10,25,26]. Main differences among our samples are limited to the cyano groups. Considering this last species, an interesting point is the presence of two species peaking at 2141 and 2176 cm^{-1}. The first is constant through the samples of the series (including the Pt/gC_3N_4) and thus it is not related to the alkali presence, and a "difference spectrum" (using Pt/gC_3N_4 as background) allows the quantification of the second species. The integrated intensity of the subtraction is presented in Fig. 5E for the different catalysts. The corresponding slopes show that K generates a factor of ca. 3.1 times more surface cyano species (per atom) than Na. This may result from the different chemical nature of the precursor salts in the K/Na cases. The formation of (alkali-associated) cyano groups was explained previously as a result of the transformation of terminal amine (NH_2) groups in cyano groups by reaction of the first with OH^- or other reactive species generated by the decomposition of the alkali precursors [27].

As the detection of the K and Na activity maxima at different molar concentrations does not apparently fit with the similar physico-chemical behavior of the series of samples, in Fig. 5F we plotted the quantum efficiency versus the cyano surface group number (measured using infrared, Fig. 5E) we observed that the region of maximum activity corresponds to a specific surface density of the mentioned surface group. This appears independent of the illumination source and alkali nature and is thus a general result describing the photo-production of hydrogen for alkali-doped carbon nitride samples. The electron capture capability

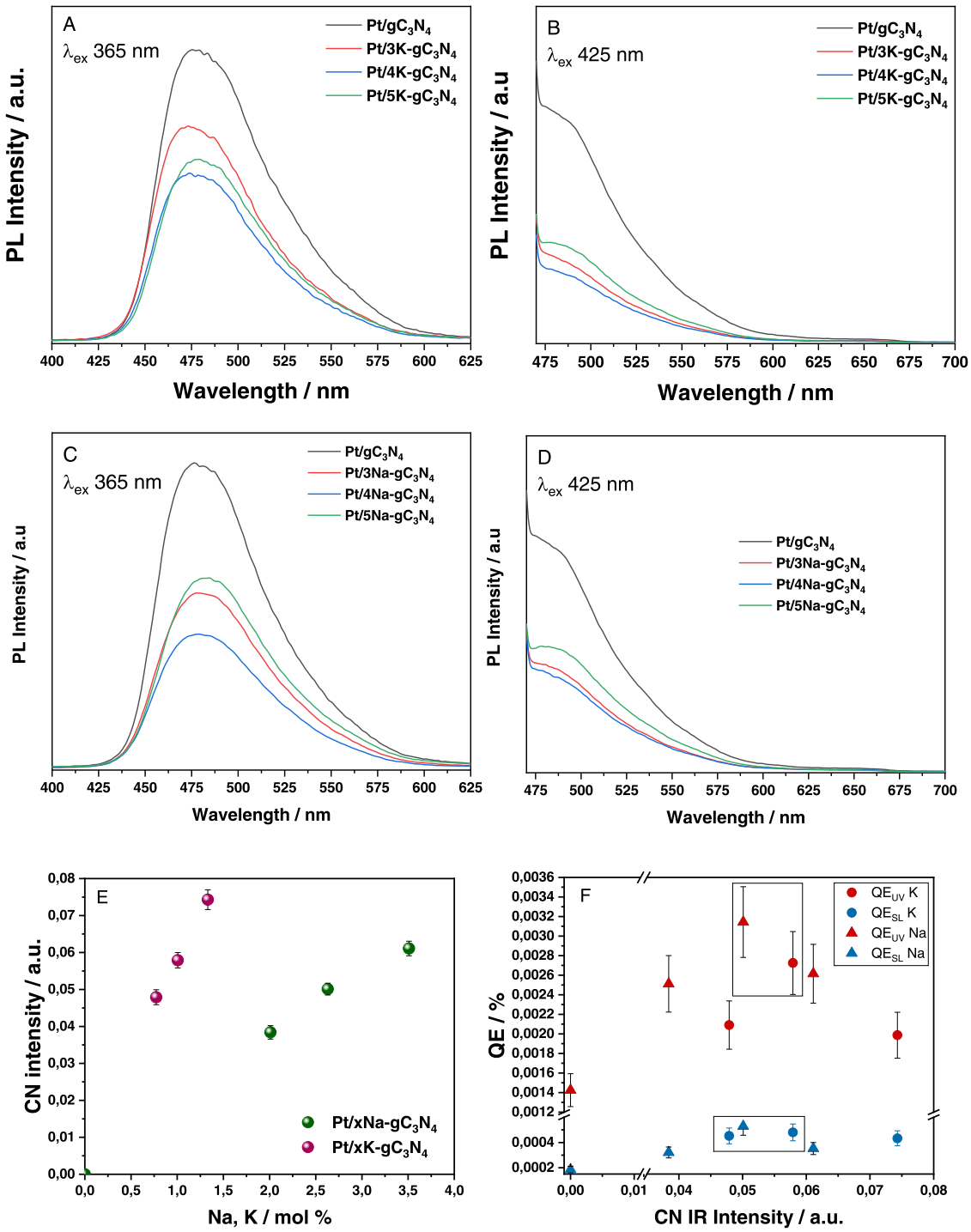

Fig. 5. (A-D) Photoluminescence spectra of Pt/X-gC_3N_4 (X = K,Na) and reference materials for two (UV, visible) excitation wavelengths. (E) Intensity of the cyano group IR band as a function of the (real) K/Na content of the materials. (F) Correlation plot between quantum efficiency and alkali-related cyano group quantity measured using infrared spectroscopy. Results for UV and sunlight-type (SL) illumination conditions are presented. Rectangles highlight zones of maximum activity.

of the cyano groups directly generated by the presence of alkali ions at the support [10,25] seems critical to enhance the photo-activity of the Pt/gC_3N_4 reference system. As recently demonstrated by Durrant's group, long lived electrons are essential to drive photo-production of hydrogen in carbon nitride based systems, although excessive accumulation would result in accelerated recombination losses and lower performance [28]. This explains the presence of a maximum in a specific region of surface cyano group concentration. Maximum activity occurs at an optimum concentration of the surface cyano group, independently of light wavelength and alkali cation nature. After this optimum concentration, the interaction between cyano entities is detrimental for activity, likely by the negative energetic effects of localizing charge close to each other. Note that the optimum concentration of cyano group occurs at different nominal (and real) concentration of the alkali promoter.

4. Conclusions

This work reports the preparation of K and Na containing carbon nitride based semiconductors. They were used jointly with a Pt co-

catalyst for the photo-production of hydrogen. The physico-chemical characterization of the solids provides evidence at alkali cations are located at bulk (interlayer) positions of the materials and that Na content of the materials is significantly higher than that of K (2.6 times for the samples prepared using equal initial molar concentration). In spite of the different alkali loadings, the series of samples displayed rather similar physico-chemical properties in terms of the structural, morphological and electronic properties of the carbon nitride and noble metal components. Main differences among samples concern the number of cyano groups originated concomitantly with the alkali incorporation to the support. K generates ca. 3.1 times more surface cyano groups per atom than Na.

The gas-phase photo-production of hydrogen was analyzed by calculating the quantum efficiency of the process. Catalysis showed stable activity under long time on stream periods. Maximum activity was achieved for samples containing different quantities of alkali ions, a 1.0 mol. % of K and 2.6 mol. % of Na. Under sunlight illumination, outstanding maximum quantum efficiency values of 2.4% and 2.8% for, respectively, K and Na series were achieved. These values indicate the suitability of the alkali incorporation to generate highly active carbon nitride based materials for solar photo-catalysis. In order to interpret activity we provided a structure-activity link. The study demonstrates for the critical role of the specific cyano groups directly connected with the presence of alkali ions in controlling activity. The optimum region of cyano surface density is identified and associated, according to literature reports, to an effective electron capture capability of these ad-species, leading to a significant decrease of charge recombination as measured using photoluminescence. This physico-chemical parameter controls the recombination of charge after illumination and thus photo-production of hydrogen irrespective of the alkali nature and illumination source, indicating the generality of the result.

CRediT authorship contribution statement

U. Caudillo-Flores: Data curation, Formal analysis, Investigation, Writing – review & editing. **A. Ares-Dorado:** Data curation, Formal analysis, Investigation, Writing – review & editing. **G. Alonso-Núñez:** Formal analysis, Investigation, Writing – review & editing. **D. Tudela:** Supervision, Formal analysis, Investigation, Writing – review & editing. **M. Fernández-García:** Funding acquisition, Project administration, Conceptualization, Investigation, Software, Supervision, Writing – review & editing. **A. Kubacka:** Funding acquisition, Project administration, Conceptualization, Investigation, Supervision, Writing – review & editing.

Declaration of Competing Interest

The authors declare that they have no known competing financial interests or personal relationships that could have appeared to influence the work reported in this paper.

Acknowledgements

Authors are thankful to “Ministerio de Ciencia e Innovación” (Spain) for supporting the work carried out through the PID2019-105490RB-C31 grant. The support by CONACyT, Mexico (SENER-CONACyT 117373) is also acknowledged by U. C.-F. M. F.G. is fully indebted to Prof. F. Fernández-Martín for general discussions. The authors thank D. A. Dominguez for obtaining XPS spectra.

Appendix A. Supporting information

Supplementary data associated with this article can be found in the online version at doi:10.1016/j.cattod.2021.06.028.

References

[1] S. Cao, J. Low, J. Yu, M. Jaroniec, Polymeric photocatalysts based on graphitic carbon nitride, Adv. Mater. 27 (2015) 2150–2176.
[2] G. Mamba, A.K. Mishra, Graphitic carbon nitride (g-C_3N_4) nanocomposites: a new and exciting generation of visible light driven photocatalysts for environmental pollution remediation, Appl. Catal. B Environ. 198 (2016) 347–377.
[3] U. Caudillo-Flores, M.J. Muñoz-Batista, R. Luque, M. Fernández-García, A. Kubacka, g-C_3N_4/TiO_2 composite catalysts for the photo-oxidation of toluene: chemical and charge handling effects, Chem. Eng. J. 378 (2019), 122228.
[4] C. Yanjuan, W. Yuxiong, W. Hao, C. Fangyan, Graphitic carbon nitrides: modifications and applications in environmental purification, Prog. Chem. 28 (2016) 428–437.
[5] M.J. Muñoz-Batista, A. Kubacka, M. Fernandez-Garcia, Effect of g-C_3N_4 loading on TiO_2-based photocatalysts: UV and visible degradation of toluene, Catal. Sci. Technol. 4 (2014) 2006–2015.
[6] N. Cheng, J. Tian, Q. Liu, C. Ge, A.H. Qusti, A.M. Asiri, A.O. Al-Youbi, X. Sun, Au-nanoparticle-loaded graphitic carbon nitride nanosheets: green photocatalytic synthesis and application toward the degradation of organic pollutants, ACS Appl. Mater. Interfaces 5 (2013) 6815–6819.
[7] W.-J. Ong, L.-L. Tan, S.-P. Chai, S.-T. Yong, Heterojunction engineering of graphitic carbon nitride (gC_3N_4) via Pt loading with improved daylight-induced photocatalytic reduction of carbon dioxide to methane, Dalton Trans. 44 (2015) 1249–1257.
[8] J.C. Colmenares, A. Magdziarz, M.A. Aramendia, A. Marinas, J.M. Marinas, F. J. Urbano, J.A. Navio, Influence of the strong metal support interaction effect (SMSI) of Pt/TiO_2 and Pd/TiO_2 systems in the photocatalytic biohydrogen production from glucose solution, Catal. Commun. 16 (2011) 1–6.
[9] K. Jiang, L. Zhu, Z. Wang, K. Liu, H. Li, J. Hu, H. Pan, J. Fu, N. Zhang, X. Qiu, Plasma-treatment induced H_2O dissociation for the enhancement of photocatalytic CO_2 reduction to CH_4 over graphitic carbon nitride, Appl. Surf. Sci. (2019), 145173.
[10] G. Liu, L. Shi, S. Yan, L. Yao, The improvement of photocatalysis H_2 evolution over g-C_3N_4 with Na and cyano-group co-modification, Front. Chem. 7 (2019) 639.
[11] S.E. Braslavsky, A.M. Braun, A.E. Cassano, A.V. Emeline, M.I. Litter, L. Palmisano, V.N. Parmon, N. Serpone, Glossary of terms used in photocatalysis and radiation catalysis (IUPAC Recommendations 2011), Pure Appl. Chem. 83 (2011) 931–1014.
[12] G.K. Williamson, W.H. Hall, X-ray line broadening from filed aluminium and wolfram, Acta Met. 1 (1953) 22–31, https://doi.org/10.1016/0001-6160(53)90006-6.
[13] P. Kubelka, New contributions to the optics of intensely light-scattering materials. Part I, J. Opt. Soc. Am. 38 (1948) 448–457, https://doi.org/10.1364/JOSA.38.000448.
[14] M. Fernández-García, A. Martínez-Arias, J.C. Hanson, J.A. Rodriguez, Nanostructured oxides in chemistry: characterization and properties, Chem. Rev. 104 (2004) 4063–4104, https://doi.org/10.1021/cr030032f.
[15] D.A. Shirley, High-resolution X-ray photoemission spectrum of the valence bands of gold, Phys. Rev. B 5 (1972) 4709–4714, https://doi.org/10.1103/PhysRevB.5.4709.
[16] M.J. Muñoz-Batista, A. Kubacka, A.B. Hungría, M. Fernández-García, Heterogeneous photocatalysis: light-matter interaction and chemical effects in quantum efficiency calculations, J. Catal. 330 (2015) 154–166, https://doi.org/10.1016/j.jcat.2015.06.021.
[17] M.J. Muñoz-Batista, M.M. Ballari, A. Kubacka, O.M. Alfano, M. Fernández-García, Braiding kinetics and spectroscopy in photo-catalysis: the spectro-kinetic approach, Chem. Soc. Rev. 48 (2019) 637–682, https://doi.org/10.1039/C8CS00108A.
[18] B. Lin, H. An, X. Yan, T. Zhang, J. Wei, G. Yang, Fish-scale structured g-C_3N_4 nanosheet with unusual spatial electron transfer property for high-efficiency photocatalytic hydrogen evolution, Appl. Catal. B Environ. 210 (2017) 173–183.
[19] L. Wang, Y. Hong, E. Liu, Z. Wang, J. Chen, S. Yang, J. Wang, X. Lin, J. Shi, Rapid polymerization synthesizing high-crystalline g-C_3N_4 towards boosting solar photocatalytic H_2 generation, Int. J. Hydrog. Energy 45 (2020) 6425–6436, https://doi.org/10.1016/j.ijhydene.2019.12.168.
[20] C.D. Wagner, G.E. Muilenberg, Handbook of X-Ray Photoelectron Spectroscopy: A Reference Book of Standard Data for Use in X-ray Photoelectron Spectroscopy, Perkin-Elmer, 1979.
[21] L. Jiang, X. Yuan, Y. Pan, J. Liang, G. Zeng, Z. Wu, H. Wang, Doping of graphitic carbon nitride for photocatalysis: a reveiw, Appl. Catal. B Environ. 217 (2017) 388–406.
[22] M.J. Munoz-Batista, O. Fontelles-Carceller, M. Ferrer, M. Fernández-García, A. Kubacka, Disinfection capability of Ag/g-C_3N4 composite photocatalysts under UV and visible light illumination, Appl. Catal. B Environ. 183 (2016) 86–95.
[23] M. Wu, J. Yan, X. Tang, M. Zhao, Q. Jiang, Synthesis of potassium-modified graphitic carbon nitride with high photocatalytic activity for hydrogen evolution, ChemSusChem 7 (2014) 2654–2658.
[24] W.-J. Ong, L.-L. Tan, Y.H. Ng, S.-T. Yong, S.-P. Chai, Graphitic carbon nitride (g-C_3N_4)-based photocatalysts for artificial photosynthesis and environmental remediation: are we a step closer to achieving sustainability? Chem. Rev. 116 (2016) 7159–7329.
[25] S. Zhang, S. Song, P. Gu, R. Ma, D. Wei, G. Zhao, T. Wen, R. Jehan, B. Hu, X. Wang, Visible-light-driven activation of persulfate over cyano and hydroxyl group co-modified mesoporous gC_3N_4 for boosting bisphenol A degradation, J. Mater. Chem. A. 7 (2019) 5552–5560.
[26] O. Fontelles-Carceller, M.J. Muñoz-Batista, M. Fernández-García, A. Kubacka, Interface effects in sunlight-driven Ag/g-C_3N_4 composite catalysts: study of the

toluene photodegradation quantum efficiency, ACS Appl. Mater. Interfaces 8 (2016), https://doi.org/10.1021/acsami.5b10434.

[27] H. Yu, L. Shang, T. Bian, R. Shi, G.I.N. Waterhouse, Y. Zhao, C. Zhou, L. Wu, C. Tung, T. Zhang, Nitrogen-doped porous carbon nanosheets templated from g-C_3N_4 as metal-free electrocatalysts for efficient oxygen reduction reaction, Adv. Mater. 28 (2016) 5080–5086, https://doi.org/10.1002/adma.201600398.

[28] W. Yang, R. Godin, H. Kasap, B. Moss, Y. Dong, S.A.J. Hillman, L. Steier, E. Reisner, J.R. Durrant, Electron accumulation induces efficiency bottleneck for hydrogen production in carbon nitride photocatalysts, J. Am. Chem. Soc. 141 (2019) 11219–11229, https://doi.org/10.1021/jacs.9b04556.